

PAPER • OPEN ACCESS

Pedestal particle balance studies in JET-ILW H-mode plasmas














To cite this article: L Horvath *et al* 2023 *Plasma Phys. Control. Fusion* **65** 044003

View the [article online](#) for updates and enhancements.

You may also like

- [Understanding the physics of ELM pacing via vertical kicks in JET in view of ITER](#)
E. de la Luna, I.T. Chapman, F. Rimini et al.
- [Progress and issues in understanding the physics of ELM dynamics, ELM mitigation, and ELM control](#)
N Oyama
- [Progress on the application of ELM control schemes to ITER scenarios from the non-active phase to DT operation](#)
A. Loarte, G. Huijsmans, S. Futatani et al.

Pedestal particle balance studies in JET-ILW H-mode plasmas

L Horvath^{1,10,*} , B Lomanowski², J Karhunen^{1,3} , M Maslov¹, P A Schneider⁴ , J Simpson^{1,5} , M Brix¹, B Chapman-Oplopoiou¹ , G Corrigan¹, L Frassinetti⁶ , M Groth⁵ , K Lawson¹ , C F Maggi¹ , S Menmuir¹, R B Morales¹ , D Moulton¹, O Myatra¹ , D Nina⁷, T Pereira¹, D I Réfy⁸, S Saarelma¹ , M Vécsei⁸ 
and JET Contributors⁹

¹ United Kingdom Atomic Energy Authority, Culham Centre for Fusion Energy, Culham Science Centre, Abingdon, Oxon OX14 3DB, United Kingdom

² Oak Ridge National Laboratory, Oak Ridge, TN, United States of America

³ VTT Technical Research Centre of Finland, PO Box 1000, Espoo, 02044 VTT, Finland

⁴ Max-Planck-Institut für Plasmaphysik, Boltzmannstrasse 2, D-85748 Garching, Germany

⁵ Aalto University, 02150 Espoo, Finland

⁶ Division of Fusion Plasma Physics, KTH Royal Institute of Technology, Stockholm, Sweden

⁷ Instituto de Plasmas e Fusão Nuclear, Instituto Superior Técnico, Universidade Lisboa, Lisboa, Portugal

⁸ Center for Energy Research, Budapest 1121, Hungary

E-mail: lhovath@pppl.gov

Received 30 September 2022, revised 20 January 2023

Accepted for publication 10 February 2023

Published 3 March 2023



CrossMark

Abstract

JET-ILW type I ELMy H-modes at 2.5 MA/2.8 T with constant NBI heating (23 MW) and gas fuelling rate were performed, utilising edge localised mode (ELM) pacing by vertical kicks and plasma shaping (triangularity, δ) as tools to disentangle the effects of ELMs, inter-ELM transport and edge stability on the pedestal particle balance. In agreement with previous studies, the pedestal confinement improves with increasing δ , mostly due to a significant increase in pedestal density while the ELM frequency (f_{ELM}) is decreased. Improved pedestal confinement with increasing δ was observed even when the pedestal MHD stability was degraded artificially by vertical kicks, implying that increased triangularity may favourably affect the inter-ELM pedestal recovery. The workflow developed to quantify the pedestal particle balance uses high time-resolution profile reflectometry to characterise the inter-ELM evolution of the plasma particle content (dN/dt), the NEO drift-kinetic solver to evaluate the neoclassical fluxes and interpretative EDGE2D-EIRENE simulations to estimate the edge particle source. The edge particle source is then constrained by deuterium Balmer- α line intensity measurements in the main chamber, which are, however, strongly affected by reflections from the metal walls. The reflections are accounted for by the CHERAB code taking the divertor emission (the brightest light source in the torus) distribution from imaging spectroscopy measurements as input. Our

⁹ See the author list of ‘Overview of JET results for optimising ITER operation’ by Mailloux *et al* 2022 *Nucl. Fusion* **62** 042026.

¹⁰ Present affiliation: Princeton Plasma Physics Laboratory, Princeton, NJ 08543, United States of America

* Author to whom any correspondence should be addressed.



Original Content from this work may be used under the terms of the [Creative Commons Attribution 4.0 licence](https://creativecommons.org/licenses/by/4.0/). Any further distribution of this work must maintain attribution to the author(s) and the title of the work, journal citation and DOI.

analysis shows that in the second half of the ELM cycle, the volume-integrated particle source is larger than dN/dt , indicating that transport plays a key role in the inter-ELM pedestal recovery.

Keywords: JET-ILW, H-mode, pedestal, particle transport, EDGE2D-EIRENE, EIRENE, fuelling

(Some figures may appear in colour only in the online journal)

1. Introduction

In an H-mode plasma [1] the confinement is improved due to the formation of a narrow transport barrier at the edge. Inside the transport barrier, the energy and particle transport are reduced, and a steep pressure gradient is formed, which gives rise to a pressure pedestal. The heightened edge pressure also leads to improved global confinement due to core profile stiffness [2–5]. However, the steep pressure gradient can trigger edge localised modes (ELMs) [6], followed by a transient loss of energy and particles which are deposited onto the plasma facing components. Understanding pedestal physics is essential to predict and optimise plasma performance in current and future tokamak experiments.

The H-mode pedestal is governed by at least three interacting processes: pedestal stability, transport and sources. The stability of the pedestal in a type I ELMy regime [6] is generally described by MHD theory [7]. The high pressure gradient and the edge current density at the edge drive Peeling-Ballooning (P-B) modes unstable [8, 9], triggering an ELM. P-B stability provides an ultimate limit on the pedestal pressure at the onset of the ELM, but the inter-ELM turbulent [10–12] and neoclassical [13, 14] transport, along with the sources, will determine the relative contributions from the pedestal density and temperature. The exact role of the edge particle source and pedestal transport in setting the density pedestal is still an open question [15]. Reduced pedestal models [16–20] have proven successful in predicting the pedestal electron pressure for a wide range of plasma scenarios, but they lack a first principle based, predictive model for the edge density.

In this study, we investigate the balance of particle sources and transport in the latter part of the ELM cycle where the pedestal recovery is typically slow compared to the transient crash and fast recovery phase [21, 22]. The evolution of the pedestal particle content is evaluated from detailed analysis of high resolution profile reflectometry data. The edge particle source is estimated by means of interpretative edge-scrape-off-layer (edge-SOL) fluid transport simulations using the EDGE2D-EIRENE code [23–25]. Comparison of these results allows an assessment of the contributions of sources and transport to edge particle balance. The role of MHD stability in the pedestal formation is also investigated.

The paper is organised as follows. Section 2 describes the analysed JET-ILW H-mode experiments and presents the comparison of pedestal density and temperature profiles. The analysis of the linear ideal MHD stability of the investigated pedestals is discussed in section 3. The interpretative EDGE2D-EIRENE simulations to estimate the edge particle source is presented in section 4. The results on the balance of the source

and transport during the inter-ELM pedestal evolution is discussed in section 5, followed by the conclusions in section 6.

2. Experiments

In this work, we investigate JET-ILW type I ELMy H-mode experiments that utilised plasma shaping (triangularity) and ELM pacing by vertical kicks as tools to disentangle the effects of edge stability, ELMs, and inter-ELM particle transport on the pedestal particle balance. It has been observed in several tokamak experiments, that the pedestal confinement typically improves with increasing triangularity [22, 26–35]. In JET and ASDEX Upgrade, the increase of pedestal pressure with triangularity, at otherwise fixed engineering parameters, is due to higher pedestal density being obtained for similar pedestal temperature [22, 26–29, 31, 32]. It has also been reported from these two devices that the ELM frequency is reduced at higher triangularities [22, 26, 30, 31]. One proposed explanation for the beneficial effect of triangularity is the improved stability of P-B modes before the ELM event (pre-ELM) [8, 36–38]. Increased triangularity decouples peeling and ballooning modes opening up second stability access leading to a higher stability boundary.

The application of a fast and controlled vertical plasma motion (known as vertical kicks in JET) for frequency control of ELMs has been successfully demonstrated on several tokamaks [39–42]. This method on JET relies on the vertical stabilization control system to drive the fast vertical plasma motion. Vertical kicks can trigger ELMs by introducing an intermittent, local perturbation of the current density close to the separatrix. If the current perturbation is large enough to destabilise the peeling component of the edge instability responsible for the ELM onset, an ELM is triggered before the pedestal would naturally reach the P-B stability limit [39].

Comparative type I ELMy H-modes were performed at 2.5 MA plasma current and 2.8 T toroidal magnetic field with constant NBI (Neutral Beam Injection) power of 23 MW, no Ion Cyclotron Resonance Heating (ICRH) in the main heating phase¹¹ and constant deuterium gas fuelling rate at 4.4×10^{22} electron s^{-1} . A lower triangularity ($\delta = \delta_{\text{lower}}/2 + \delta_{\text{upper}}/2 = 0.2$) and a higher triangularity ($\delta = 0.3$) pulse with natural ELM frequency and a higher triangularity ($\delta = 0.3$) pulse with 36 Hz vertical kicks for ELM pacing were selected

¹¹ RF was not used in the main heating phase (which is the plasma analysed), but was used in the tail of the discharge for safe landing, to prevent disruption caused by core tungsten accumulation and thus radiative collapse during the plasma current ramp-down.

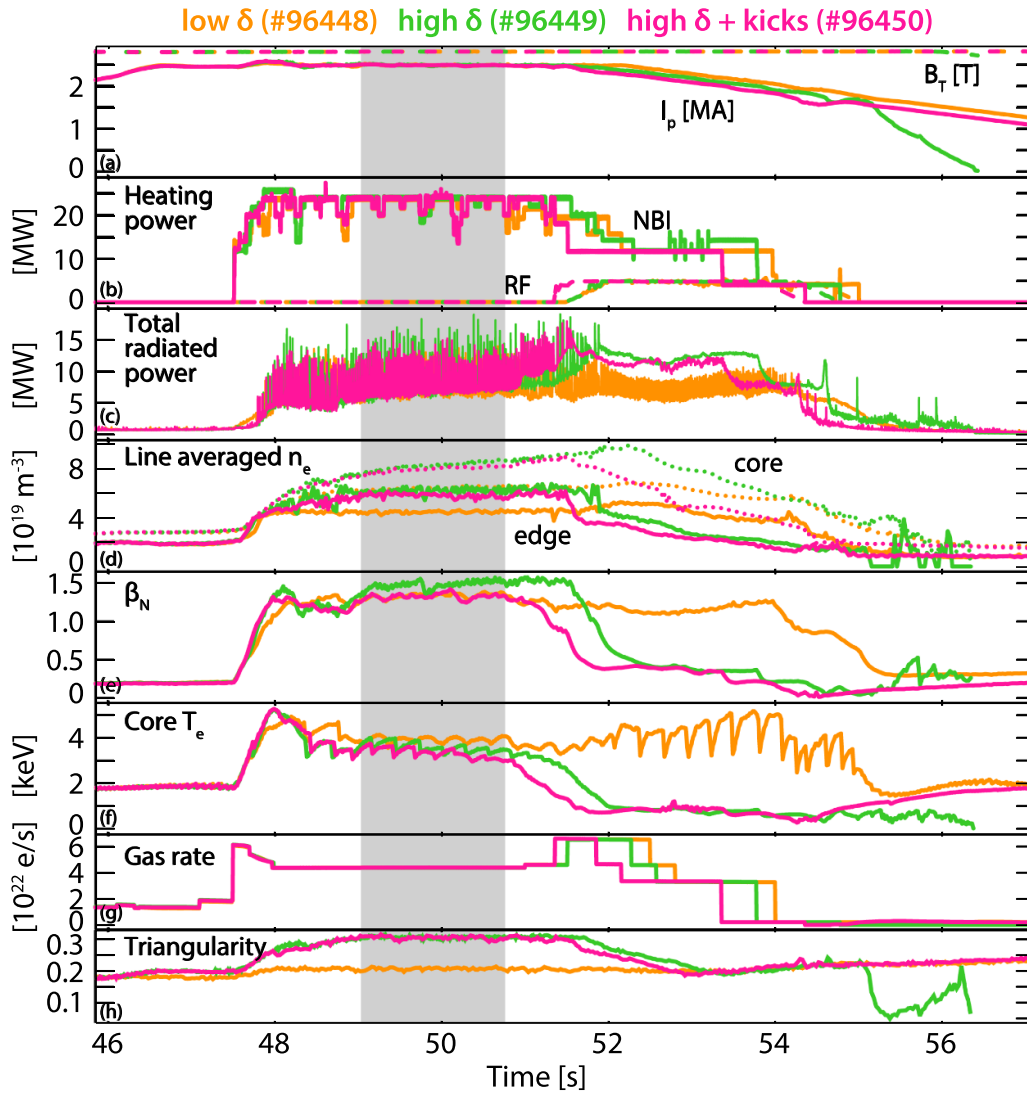


Figure 1. The main plasma parameters of the three representative discharges examined in this paper. The $\delta = 0.2$ plasma is shown in orange, the $\delta = 0.3$ in green and the $\delta = 0.3$ with kicks in magenta. The grey area indicates the analysed time interval. (a) The total plasma current, I_p and the toroidal magnetic field, B_t . (b) The NBI and ICRH heating power. (c) The total radiated power. (d) The core and edge line averaged density. (e) The normalised plasma β , β_N . (f) The core electron temperature. (g) The external D_2 fuelling gas rate. (h) The average plasma triangularity, $\delta = \delta_{\text{lower}}/2 + \delta_{\text{upper}}/2$.

for detailed comparative analysis. The main waveforms of these three pulses are shown in figure 1. Strike point sweeping with 4 Hz frequency was introduced in these pulses for operational reasons, to reduce the heat load on the tungsten coated divertor tiles. This introduces oscillations in some of the measured plasma parameters.

The pedestal electron density (n_e) and temperature (T_e) profiles from Thomson scattering (TS) [43] and the ion temperature (T_i) profiles from the edge charge exchange spectroscopy (CXRS) system [44, 45] measuring Ne and C impurities are shown in figure 2. These figures show all of the TS and CXRS profiles from the steady phase of the discharge, i.e. including both ELMs and inter-ELM phases. Besides the raw data points, figure 2 shows the modified tanh (mtanh) [46] fitted profiles as well. Figure 2(c) also shows the raw ion temperature data on the top of the mtanh fit of the electron temperature profiles

(same as in figure 2(b) for comparison of T_e and T_i). The ion and electron temperatures are similar at the pedestal top within the measurement uncertainties of the edge CXRS system, but T_i in the edge transport barrier and at the separatrix cannot be resolved.

As shown in figure 2, the pedestal pressure significantly improves with increasing triangularity mostly due to an increase in pedestal density and the change in electron and ion temperatures is small. Also, the natural ELM frequency decreases from 39 Hz at $\delta = 0.2$ to 25 Hz at $\delta = 0.3$. When f_{ELM} is increased by vertical kicks at $\delta = 0.3$ to 37 Hz (close to the natural f_{ELM} of the $\delta = 0.2$ pulse), the pedestal density and thus the pressure is somewhat decreased, but both still significantly higher than in the $\delta = 0.2$ case. This observation is discussed in view of the pedestal stability in the next section.

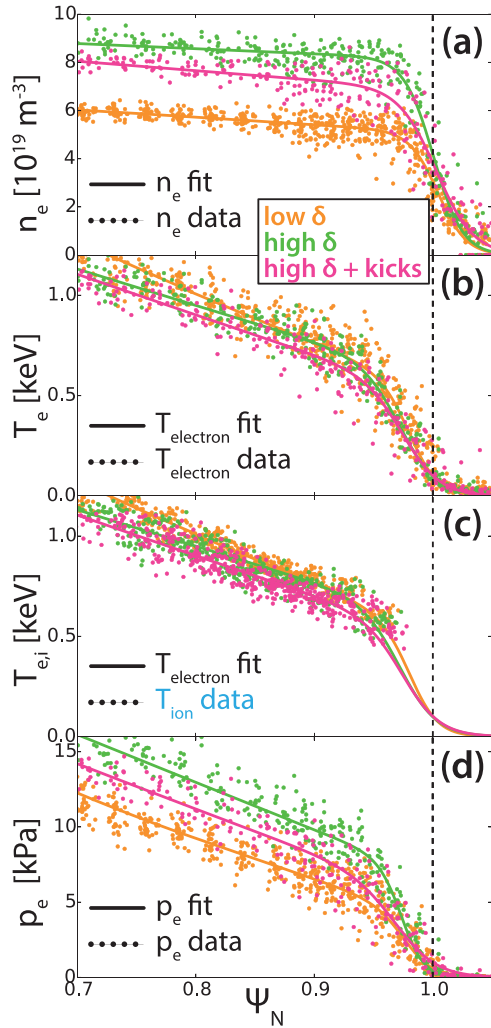


Figure 2. The pedestal kinetic profiles for the three representative discharges examined in this paper. These figures show all of the TS and CXRS profiles from the steady phase of the discharge, i.e. including both ELMs and inter-ELM phases. The $\delta = 0.2$ plasma is shown in orange, the $\delta = 0.3$ in green and the $\delta = 0.3$ with kick in magenta. (a) Electron density data from TS and corresponding mtanh fits. (b) Electron temperature data from TS and corresponding mtanh fits. (c) Ion temperature data from CXRS. The underlying solid lines are the mtanh fits of the TS electron temperature, same as in figure (b). This is to confirm that $T_e \approx T_i$ at the pedestal top. (d) Electron pressure data from TS and corresponding mtanh fits. (The kinetic profiles are radially aligned so that the separatrix temperature is 100 eV).

3. Pedestal MHD stability

Vertical kicks can help to investigate whether physics mechanisms other than improved P-B stability play a role in the observed increase in pedestal performance at higher triangularity. With the introduction of vertical kicks, the ELMs are triggered before the pedestal would naturally reach the MHD stability limit. In the $\delta = 0.3$ plasma with vertical kicks, the pedestal pressure is degraded (by $\approx 25\%$) with respect to the $\delta = 0.3$ discharge with natural f_{ELM} . Despite this artificial degradation of the pedestal MHD stability, the pedestal pressure is still significantly higher (by $\approx 30\%$) in the $\delta = 0.3$

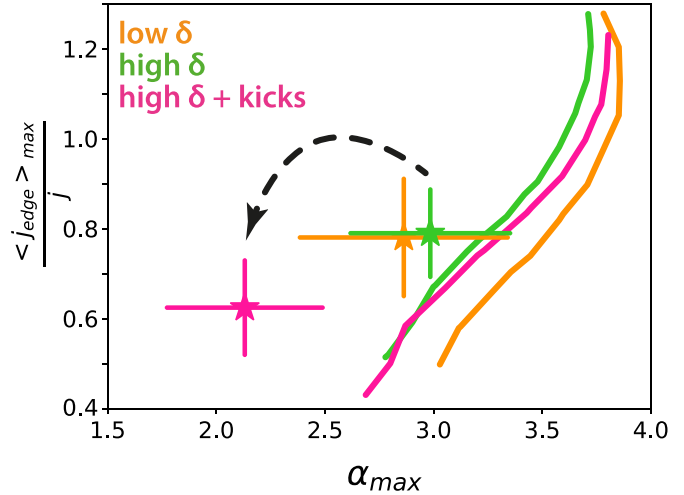


Figure 3. Linear MHD pedestal stability diagram for the three discharges analysed. The $\delta = 0.2$ plasma is shown in orange, the $\delta = 0.3$ in green and the $\delta = 0.3$ with kick in magenta. The operational points corresponding to the pre-ELM phase of the discharges are indicated with the stars and the respective error bars as a function of the normalised pressure gradient (α_{max}) and the normalised current density ($\langle j_{\text{edge}} \rangle_{\text{max}} / j$). The solid lines show the P-B stability boundary.

kicked pulse compared to that of the $\delta = 0.2$ counterpart. This implies that increased plasma triangularity may also affect inter-ELM transport, and thus lead to increased pedestal confinement.

Ideal MHD stability of the pedestal was investigated with the HELENA fixed boundary equilibrium [47] and the ELITE ideal MHD stability codes [8, 9]. The $j - \alpha$ pedestal stability diagram for the three representative discharges is shown in figure 3, where α is the normalised pressure gradient¹² and j is the normalised current density. The HELENA equilibrium is self-consistent with respect to the current profile that was evaluated using Redl's bootstrap current formula [49] and assuming a fully diffused Ohmic current with neoclassical resistivity. The pre-ELM (80%–97%)¹³ mtanh fitted TS data was used as input kinetic profiles, assuming $T_e = T_i$ (consistent with charge exchange measurements at the pedestal top) and line averaged Z_{eff} with Be as a single impurity. The kinetic profiles are radially aligned so that the separatrix temperature is 100 eV.

The P-B stability boundary (solid lines in figure 3) was evaluated using $\gamma_{\text{MHD}} > 0.5 \times \omega_{\text{dia}}$ as stability criterion, where γ_{MHD} is the linear growth rate and ω_{dia} is the diamagnetic frequency. The stability boundary is very similar for all three

¹² The normalised pressure gradient is defined as in [48]: $\alpha = \frac{-2\partial V / \partial \Psi}{(2\pi)^2} \left(\frac{V}{2\pi^2 R_0} \right)^{1/2} \mu_0 \frac{\partial p}{\partial \Psi}$, where V is the volume enclosed by the flux surface, R_0 is the geometric centre of the plasma and Ψ is the poloidal flux.

¹³ All ELM cycles are normalised to a relative time scale, where 100% corresponds to the onset of the ELM crash and 0% corresponds to the ELM crash of the preceding ELM cycle. The pre-ELM phase is defined as the 80%–97% of the ELM cycle.

discharges and no clear stabilisation effect from higher δ can be seen. This is because the increase in triangularity from 0.2 to 0.3 is too small and other parameters of the experimental equilibria (such as β_N , β_{pol} , volume, etc) affecting the stability boundary more. In a separate study (not shown here), a small stabilising effect of triangularity was recovered when all other parameter differences between discharges were removed and only the shaping effect was investigated by increasing δ from 0.2 to 0.3.

The stars in figure 3 show the operational point of the pedestal as obtained in the experiment with their associated error bars derived from the uncertainty of the mtanh fit parameters. The operational points for the pulses with natural ELM frequency are close to the P-B boundary thus the ELM trigger is consistent with the P-B paradigm. The operational point is further from the stability boundary for the $\delta = 0.3$ pulse where vertical kicks were applied to increase f_{ELM} . This is expected as the vertical kick introduces a current perturbation at the edge which triggers the ELM in conditions when the pedestal would otherwise still be stable to P-B modes. The P-B stability analysis used the equilibrium and kinetic profiles from this stable period preceding the triggered ELMs.

It was found that the pressure pedestal is wider in both $\delta = 0.3$ pulses than in the $\delta = 0.2$ case. This is shown in figure 4, where the edge pressure gradients are compared for the three pedestals. The wider pedestal at $\delta = 0.3$ allows for improved P-B stability and thus leads to higher pedestal pressure. This suggests that the improved pedestal pressure at higher δ is not necessarily a sole pre-ELM P-B stability effect, but a change in inter-ELM transport could possibly play an important role in setting the higher density and thus higher pressure when the triangularity is increased.

4. Estimate of the edge particle source

The role of particle transport in the inter-ELM phase is studied in section 5 in more detail where the pedestal particle balance is discussed. In this section, we present the interpretative EDGE2D-EIRENE [23–25] simulations which were performed to estimate the edge particle source to examine the balance of source and transport in the pedestal. EDGE2D is a 2D fluid code with realistic geometry of the SOL and divertor region, which is coupled to EIRENE, a Monte Carlo code used to calculate the neutral particle distribution.

4.1. Simulation set-up and interpretative transport coefficients

We ran EDGE2D-EIRENE in interpretative mode, where the perpendicular transport coefficient of electron particle diffusion D_{\perp} ($\Gamma_{e,\perp} = D_{\perp} \nabla_{\perp} n_e$), electron and ion heat transport $\chi_{e,i,\perp}$ ($q_{e,i,\perp} = -n_{e,i} \chi_{e,i,\perp} \nabla_{\perp} T_{e,i}$) and the divertor pump albedo were iterated until the solution fitted the measured inter-ELM (40–80% fraction of the ELM cycle) upstream n_e and T_e profiles (measured by TS and the fast Li-beam emission spectroscopy system [50]). The ion and electron heat transport coefficient profiles ($\chi_{e,\perp}$ and $\chi_{i,\perp}$) were assumed

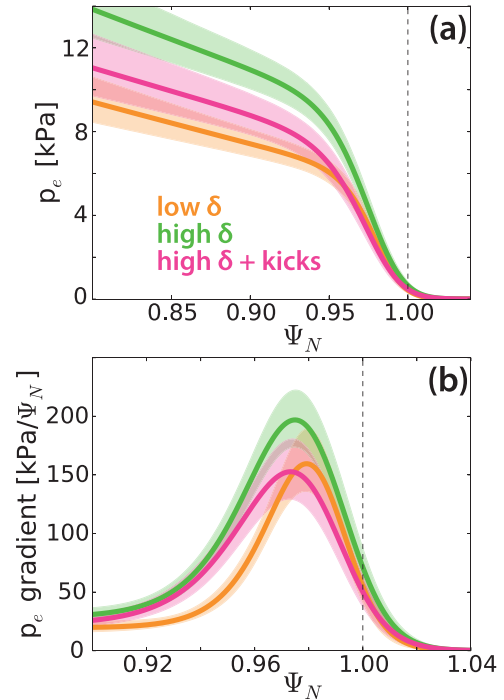


Figure 4. The mtanh fit of the pre-ELM (80%–97%) electron pressure profile (a) and its gradient (b) for the three discharges analysed. The $\delta = 0.2$ plasma is shown in orange, the $\delta = 0.3$ in green and the $\delta = 0.3$ with kick in magenta. The error bars are derived from the uncertainty of the mtanh fit parameters. Note that while the pressure gradient is similar for the $\delta = 0.2$ and the $\delta = 0.3$ with kicks cases, α as shown in figure 3 is different. This is because the normalisation of the pressure gradient (α) also includes the plasma volume that is smaller for the $\delta = 0.3$ plasmas.

to be the same, due to lack of constraints to distinguish between them.

The separate contribution of ELM and inter-ELM transport was not studied with EDGE2D-EIRENE. The simulations were run until convergence, thus time independent solutions were obtained. The building up of the plasma stored energy between ELMs (dW/dt), that is equivalent to the ELM power loss (P_{ELM}), was not taken into account in the time-independent simulations. Thus, the input power in EDGE2D-EIRENE was set to the power crossing the separatrix inter-ELM ($P_{inter-ELM} = P_{sep} - P_{ELM}$).

Cross-field drifts and a particle pinch term were not introduced in these simulations. The edge particle pinch may have an important role in the particle transport [51–53], but in time independent simulations the experimental n_e profile could be reproduced with different variations of the diffusion coefficient and the pinch velocity, due to the lack of constraints. Thus, the particle diffusion coefficient here is regarded as an effective parameter describing the transport needed to exhaust the particle source from the plasma.

The grid for EDGE2D is generated such that it is aligned to the plasma equilibrium reconstructed using kinetic EFIT [54]. The grid extends to ~ 10 – 15 cm inside the separatrix towards the core plasma. The gas fuelling rate and location was set in accordance with the experiment. The recycling coefficient

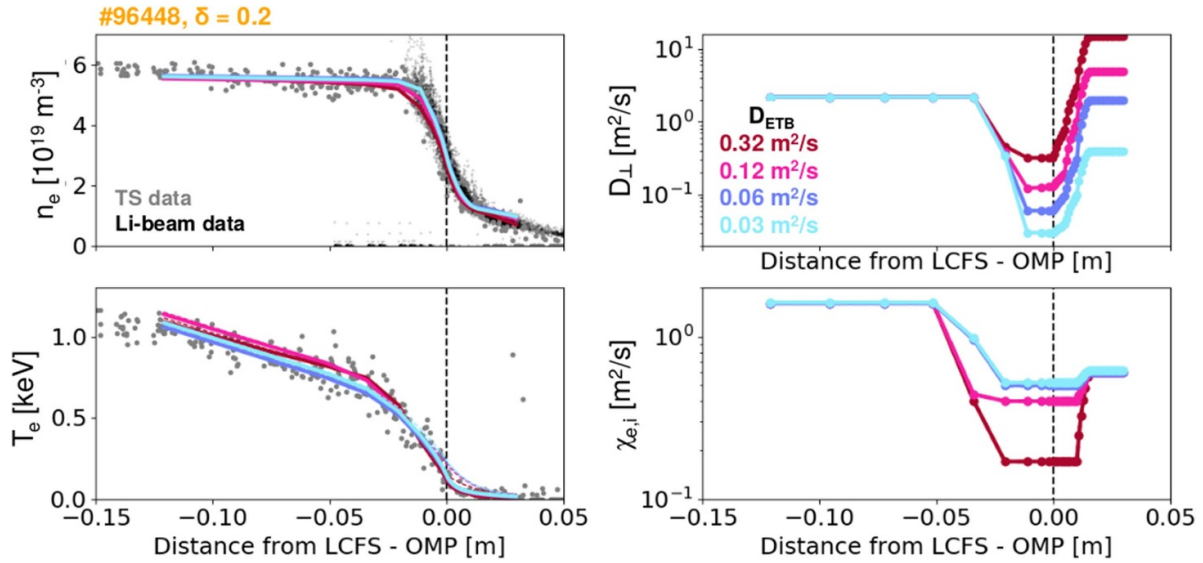


Figure 5. Inter-ELM TS profiles for n_e and T_e (in grey) and Li-BES data for n_e in the SOL (in black) in the steady phase of the $\delta = 0.2$ discharge. The upstream n_e and T_e profiles of the interpretative EDGE2D-EIRENE simulations with different set of D_{\perp} coefficients are shown in colour. The simulations are labelled with the corresponding D_{\perp} value inside the edge transport barrier, $D_{\perp,ETB}$.

was set to 1 on the walls and the divertor targets¹⁴. The experimental NBI fuelling rate was estimated using the PENCIL code [55], although this was found to be small compared to the neutral flux crossing the separatrix. The divertor configuration around the outer strike point cannot be modelled precisely in EDGE2D-EIRENE. The wall structure had to be slightly modified around the outer strike-point so that the grid does not cross wall surfaces, as described in [56] in more detail.

4.2. EDGE2D-EIRENE solutions

As described above, the perpendicular transport coefficients were iterated until the experimental upstream kinetic profiles could be matched. However, it has been found that multiple sets of transport coefficients can reproduce the kinetic profiles within the experimental uncertainty without simultaneously constraining the main chamber recycling. This is shown in figure 5, where the transport coefficients and the corresponding upstream n_e and T_e profiles are shown for the $\delta = 0.2$ discharge. For these four simulations, all the input parameters were kept the same except for the perpendicular transport coefficients. It is shown in figure 5, that the particle diffusion coefficient changes by an order of magnitude in the pedestal and the SOL, while the heat transport coefficient changes by a factor of 3 in the pedestal. Regardless of this significant variation in the perpendicular transport, the upstream profiles

remain almost unchanged. It is important to note that the divertor target quantities did not vary significantly either in this scan. The variation in j_{sat} , n_e and T_e at the outer target was between $\pm 30\%$. For the inner target, the highest D_{\perp} case is significantly colder than the other three cases. j_{sat} , n_e and T_e for the three lower D_{\perp} cases, however, are also within $\pm 30\%$ variation.

The above behaviour can be understood by examining the role of main chamber recycling in fuelling the plasma. The recycling flux is determined by ion flux arriving to the edge of the EDGE2D plasma grid. The recycling coefficient was set to 1 in these simulations (except for the pumping surfaces in the divertor), thus all particles are recycled as neutrals. By increasing the particle diffusion coefficient, the ion flux arriving at the edge of the plasma and at the wall surfaces is also increased, resulting in a higher recycling flux. The increased recycling flux leads to a higher neutral density and such increased particle source and it is this increased particle source in the plasma that compensates the effect of increased particle transport. In this way, multiple sets of particle diffusion coefficients can reproduce very similar upstream kinetic profiles.

It is therefore necessary to also constrain the main chamber particle source, so as to extract the unique set of D_{\perp} and χ_{\perp} profiles that matches the investigated pedestal. Figure 6 shows the ionisation source inside the separatrix as a function of $D_{\perp,ETB}$ for the four simulations presented in figure 5. It can be seen that for these cases, the pedestal source increase approximately linearly with $D_{\perp,ETB}$ resulting in similar upstream density and temperature profiles (as shown in figure 5) despite different set of transport coefficients. This also means that additional simulation constraints that carry information on the

¹⁴ The projection algorithm used for main chamber recycling assumes that all of the ion flux arriving at the edge of the plasma grid is being recycled at the wall. The effect of this choice on the simulation results is discussed in section 6.

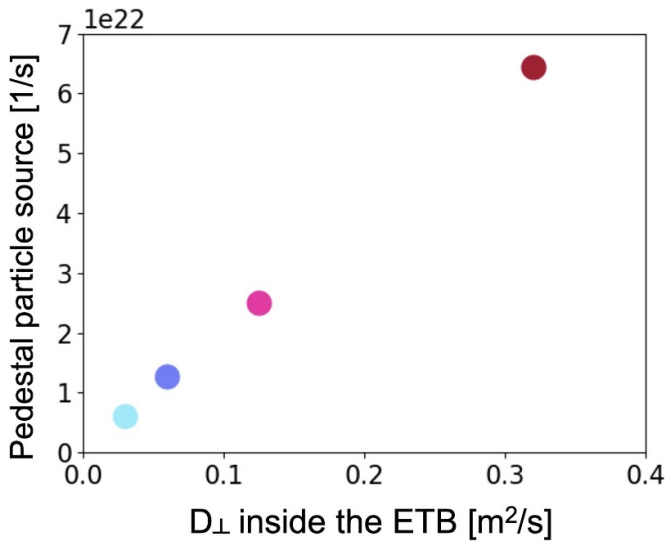


Figure 6. The particle source integrated over the plasma volume inside the separatrix is shown as a function of $D_{\perp, \text{ETB}}$ inside the edge transport barrier (ETB) for the four interpretative EDGE2D-EIRENE simulations with different set of D_{\perp} coefficients (#96448, $\delta = 0.2$).

neutral density in the main chamber are needed to estimate the pedestal particle source.

4.3. Main chamber D_{α} line radiation constraint in EDGE2D-EIRENE

In order to constrain the pedestal particle source, we compared the emitted deuterium Balmer- α (D_{α}) radiation by the main chamber plasma in the EDGE2D-EIRENE simulation to that of the experimental measurements. The line-of-sight (LOS) of the corresponding spectrometer crosses the plasma in the main chamber, but not in the divertor as shown in figure 7(c). In this way, the measured line intensity carries direct information about the ionisation source in the SOL and the pedestal, but it does not integrate through the orders of magnitude brighter divertor emission. However, the D_{α} emission from the divertor is reflected by the JET-ILW metallic walls [57], hence it is captured along the horizontal LOS making significant contribution to the measured line intensity. Thus reflections need to be taken into account in the analysis by forward modelling.

To estimate the effect of reflections on the measured signal, the experimental D_{α} brightness in the divertor was taken from imaging spectroscopy measurements [58]. Imaging spectroscopy provided a time-averaged (during the inter-ELM phases over the steady phase of the discharge), 2D tomographic reconstruction of the D_{α} line intensity distribution in the divertor. The contribution of the reflected light from the divertor to the horizontal D_{α} line intensity measurement was estimated using the CHERAB code [59, 60] as illustrated in figure 7(c). CHERAB includes definitions of the full JET-ILW machine geometry and estimates of the metallic tile spectral bidirectional reflectance distribution functions. It uses the RAYSECT [61] raytracing engine to provide estimates for the reflected light intensity. We used the experimental divertor D_{α}

emission as input for CHERAB, assuming zero emission from the main chamber. In this way, the background reflected emission of the measured D_{α} intensity on the horizontal LOS can be approximated.

The measured D_{α} light intensity as function of time is shown in grey in figure 7. The difference of the measured signal and the background reflected emission provides an estimate for the line intensity emitted by the plasma in the main chamber (the SOL and the pedestal). These estimated main chamber D_{α} line intensities are shown in figures 7(a) and (b) in black for the steady phase of the $\delta = 0.2$ and $\delta = 0.3$ natural f_{ELM} discharges after removing the spikes caused by ELMs. The obtained signal is affected by large oscillations, in part due to the applied strike point sweeping, which increases the uncertainty on this method to constrain the neutral density in the plasma. Nonetheless, this experimental comparison provides a sanity check on the overall level of main chamber D_{α} emission in EDGE2D-EIRENE simulations and thus excludes some of the solutions obtained with unrealistic level of particle source in the pedestal and SOL.

To compare with the estimated experimental main chamber D_{α} line intensities, synthetic diagnostic data was produced from the EDGE2D-EIRENE solutions by evaluating (using ADAS atomic data [62]) and integrating the D_{α} emission along the diagnostic LOS. This is shown in figures 7(a) and (b) with the coloured lines. For the simulations using higher D_{\perp} values, the synthetic D_{α} emission is significantly larger than the experimental estimate for both cases. Thus, the simulations flagged as $D_{\perp, \text{ETB}} = 0.03 \text{ m}^2 \text{ s}^{-1}$ and $0.06 \text{ m}^2 \text{ s}^{-1}$ for the $\delta = 0.2$ case, and $D_{\perp, \text{ETB}} = 0.04 \text{ m}^2 \text{ s}^{-1}$ and $0.06 \text{ m}^2 \text{ s}^{-1}$ for the $\delta = 0.3$ case are the ones deemed experimentally feasible solutions.

Since the measured D_{α} emission along the horizontal LOS is dominated by reflections from the divertor, unfortunately it is not possible to select a unique solution from the EDGE2D/EIRENE simulations and thus fully constrain the evaluation of the edge particle source. Nevertheless, in the next section, we discuss the balance of the source and transport during the inter-ELM pedestal evolution in view of the above, experimentally feasible EDGE2D-EIRENE solutions with the consideration of the large uncertainty on the pedestal particle source.

5. The balance of the source and transport during the inter-ELM pedestal evolution

The main aim of this investigation is to characterise the balance of sources and transport that sets the density pedestal. In current tokamak experiments, the dominant particle fuelling in the pedestal comes from the ionisation of neutral atoms penetrating into the confined region. The dominant channels of particle transport are ELM losses, neoclassical and turbulent transport. Other loss channels, for example ion orbit losses and ripple losses, are assumed to be small. Our aim is to estimate the contribution of these different channels. For this, the transient nature of ELMs needs to be considered as well.

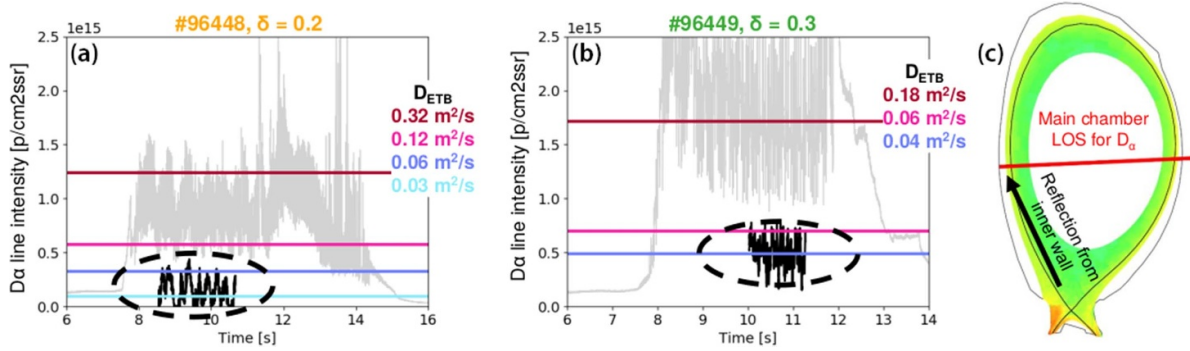


Figure 7. The measured D_α light intensity as function of time is shown in grey for the $\delta = 0.2$ and $\delta = 0.3$ natural f_{ELM} discharges. The signals after the removal of ELMs and offsetting the reflected light are shown in black. The synthetic D_α line intensities for the corresponding main chamber LOS are shown in colour from the EDGE2D-EIRENE solutions using different set of transport coefficients.

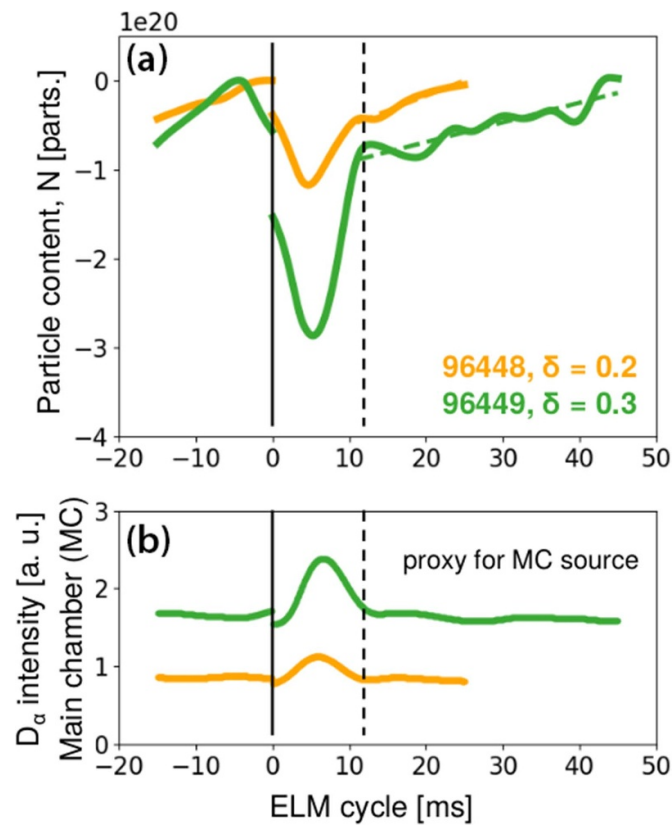


Figure 8. (a) Time evolution of the particle content during an ELM cycle (offset to 0 at the ELM onset) and (b) time evolution of the D_α light intensity in the main chamber during an ELM cycle for the low $\delta = 0.2$ and $\delta = 0.3$ natural f_{ELM} pulses.

Figure 8(a) shows the time evolution of the particle content (offset to zero at the ELM onset) evaluated from profile reflectometry during an ELM cycle for the low $\delta = 0.2$ and $\delta = 0.3$ natural f_{ELM} pulses. At the ELM crash, significant amount of particles is lost from the plasma. But most of the lost particles are quickly recovered. The start of the ELM crash is denoted by the solid black line, while the end of the ‘fast’ recovery phase is indicated with the black vertical dashed line in figure 8(a). Experimental evidence [63] suggests that the fast recovery may be driven by an increased recycling flux as a result of the increased particle flux arriving to the divertor targets and limiter as a result of the

ELM crash. A sign of this increase in particle source can be seen in the spectroscopy data in figure 8(b), where the D_α light intensity in the main chamber is shown. As discussed in section 4, the quantitative interpretation of this signal is challenging, but it shows that qualitatively the ionisation source in the main chamber is increased following the ELM crash.

The ‘fast’ recovery phase is followed by a slower and longer phase (to the right of the horizontal dashed line). In the slower recovery phase, the main chamber D_α light intensity is approximately constant. We focus on the slow recovery phase to study the pedestal particle balance assuming that the rate of change

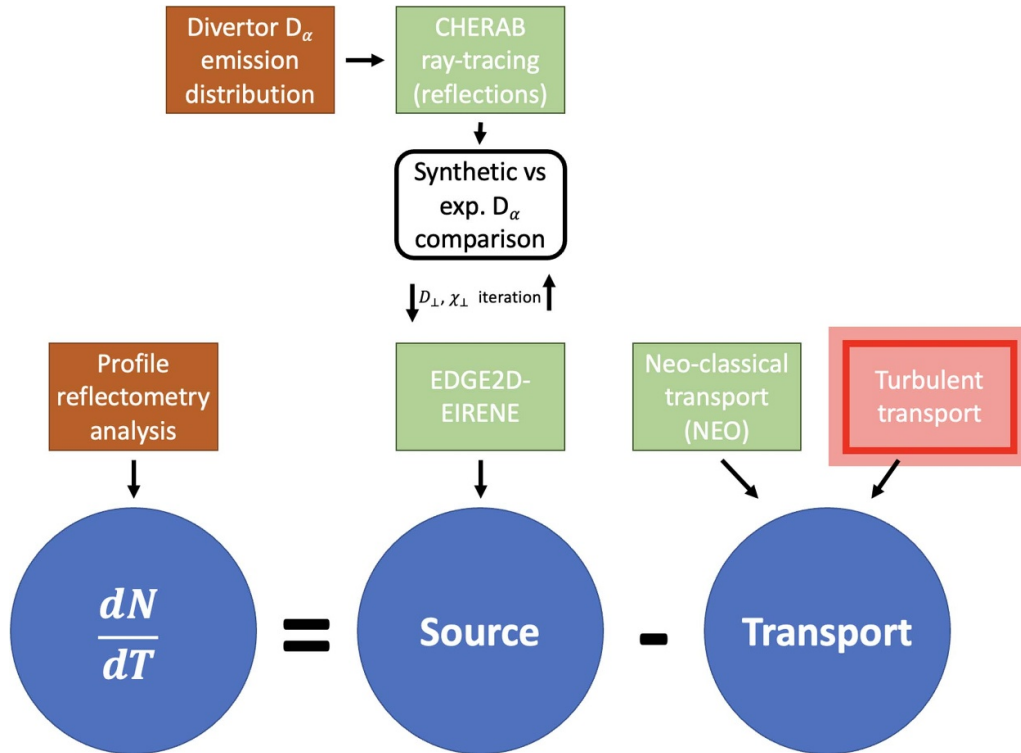


Figure 9. The analysis workflow describing the characterisation of the particle balance. The orange boxes refer to experimental data analysis, while the green boxes indicate simulations. The turbulent transport (red box) is an output in the sense that it is calculated from the other terms.

of the particle content (dN/dt) is a result of the difference between the constant source (S) and transport (T) terms:

$$dN/dt = S - T. \quad (1)$$

The question we seek to answer is to see whether the pedestal recovery is dominated by the source or the transport. To answer this question, we are combining together the data analysis procedures and simulation tools presented in previous sections. The workflow is summarised in a flowchart in figure 9. dN/dt is evaluated from the experimentally measured evolution of the particle content using high resolution profile reflectometry as explained earlier in this section. The source is taken from the experimentally relevant EDGE2D-EIRENE simulations from section 4. This requires the introduction of a simulation constrain for the main chamber D_α emission in EDGE2D-EIRENE. The main chamber D_α intensity measurement is largely affected by reflections from the divertor. The reflections are accounted for by using the CHERAB code which takes the experimental divertor D_α emission distribution as input. The magnitude of pedestal transport is then calculated as a difference between the source and dN/dt . The transport channel is then further divided into contributions from neoclassical and turbulent transport¹⁵ by estimating the neoclassical particle flux using the NEO drift-kinetic code

[64, 65]. The NEO code takes a plasma equilibrium and corresponding kinetic profiles as input and calculates the neoclassical particle and heat flux profiles as a result. The peak of the particle flux profiles in the pedestal is used in this analysis. Note that the turbulent particle flux is not modelled in this work, it is simply deduced from equation (1), assuming that the total transport (T) is the sum of the neoclassical and turbulent fluxes.

The bar charts in figure 10 compare the magnitude of the source with that of the transport for the two investigated plasmas ($\delta = 0.2$ in figure 10(a) and $\delta = 0.3$ in figure 10(b)). We show two results for both plasmas. These represent the estimated particle source from the ‘experimentally relevant’ EDGE2D-EIRENE simulations as shown in figure 7. We regard the two solutions (for each pulse) as a lower and upper bound estimate for the particle source, and the corresponding transport flux is calculated respectively using the experimentally measured dN/dt .

For the $\delta = 0.3$ pulse (figure 10(b)), it is clear that both the source and transport terms are relevant and the difference of these two large terms results in a small dN/dt . The contribution of neoclassical transport is small, $D_{NC} \approx 0.004 \text{ m}^2 \text{ s}^{-1}$ for the $\delta = 0.2$ case and $D_{NC} \approx 0.006 \text{ m}^2 \text{ s}^{-1}$ for the $\delta = 0.3$ case. This suggests that the role of turbulent transport is important in the evolution of the pre-ELM pedestal and it cannot be neglected. In the case of the $\delta = 0.2$ discharge, the picture is less clear. Due to the uncertainties on the main chamber D_α radiation constraint, the relative difference in the upper and lower bounds is greater than that of the $\delta = 0.3$ pulse.

¹⁵ Strictly speaking the transport channel is divided into neoclassical and any other transport. However, it is assumed that the latter is dominated by turbulent transport and the contribution from ion orbit losses and ripple losses is small.

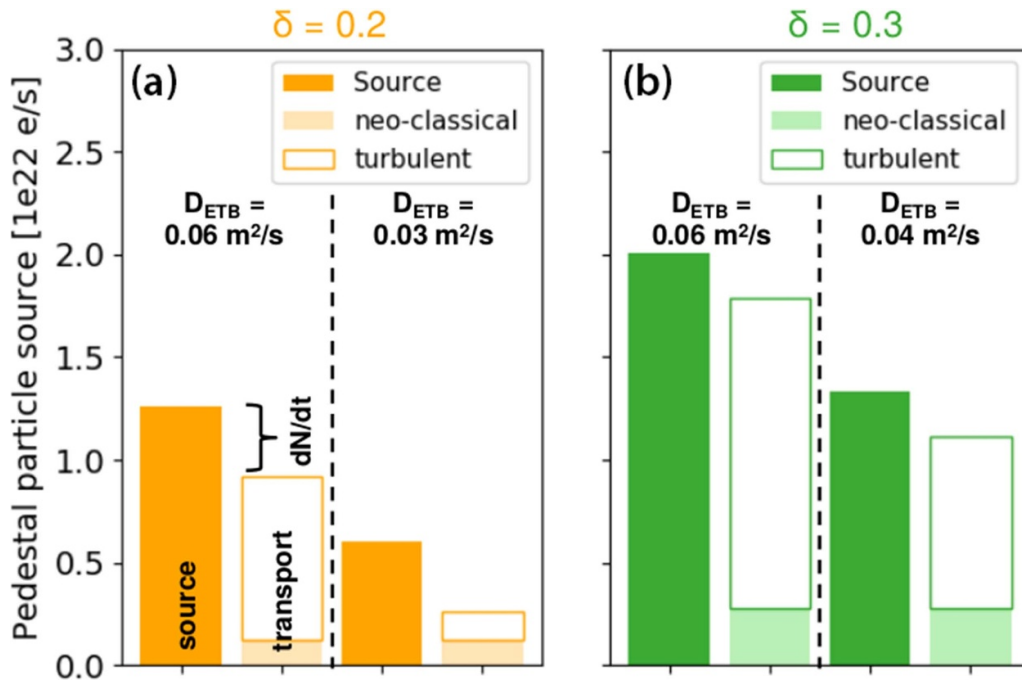


Figure 10. Comparison of the source and transport in the pedestal for the ‘experimentally relevant’ EDGE2D-EIRENE solutions for the two investigated plasmas. (a) $\delta = 0.2$ in orange, (b) $\delta = 0.3$ in green.

In the $D_{\perp,ETB} = 0.03 \text{ m}^2 \text{ s}^{-1}$ case the source seems to be dominant over transport, but in the $D_{\perp,ETB} = 0.06 \text{ m}^2 \text{ s}^{-1}$ case the source and transport terms are comparable. In summary, we conclude that the role of turbulent particle transport, in the pulses analysed, cannot be neglected from the pedestal particle balance. But, further improvements required both in spectroscopic measurements and edge transport simulations to be able to quantitatively compare the pedestal particle balance between different pedestals.

6. Discussion and conclusions

In the present paper, the pedestal particle balance and the role of pedestal MHD stability have been investigated in JET-ILW type I ELMy H-mode plasmas at different triangularities and ELM frequency. We have observed that the pedestal pressure is higher at higher δ even when the pedestal stability is artificially degraded by introducing vertical kicks, suggesting that improved P-B stability is not solely responsible for improved pedestal performance. This is likely due to the increased width of the pedestal at higher δ that allows for higher pedestal pressure at similar pressure gradient. The physical mechanism responsible for the wider pedestal has not been investigated in this work, but a change in inter-ELM pedestal transport as a result of enhanced shaping offers a candidate explanation. Unfortunately the workflow presented in this work cannot provide quantitative comparative evidence of transport between the pedestals with different triangularities as the estimate on the pedestal particle source is too uncertain.

The literature contains several gyrokinetic studies pertaining to the impact of plasma shaping on core turbulence [66–68], but we have not found any systematic study

investigating the effect of triangularity on pedestal turbulent transport. In reference [66], Belli mentions that nonlinear gyrokinetic simulations of core turbulence capture some of the shaping effects found experimentally, but they do not completely explain the degree of this dependence on triangularity. It may be that much of the experimentally observed strong triangularity dependence comes from the edge turbulence, which sets the boundary conditions for core transport.

In current tokamaks, the characterisation of the neutral source is essential to understand the formation of the density pedestal structure, as also suggested by several studies [15, 69–71]. However, due to the lack of direct measurement of the neutral density, unravelling the role of the edge particle source and transport in setting the density pedestal structure is highly challenging. In this work, we used edge-SOL transport simulations (EDGE2D-EIRENE), together with various plasma measurements for the estimation of the edge particle source. Comparing the estimated pedestal particle source with the experimentally inferred evolution of the pedestal particle content inter-ELM, we found that the role of turbulent particle transport, in general, cannot be neglected from the pedestal particle balance. Cases exist where a large source term is balanced by a large transport term resulting in a relatively slow recovery of the pedestal. This implies that for detailed pedestal prediction, the properties of both the particle source and transport need to be characterised.

The workflow presented in this study offers a way to constrain the overall magnitude of the pedestal particle source. However, the separate contribution of divertor and main chamber recycling, and external gas injection to pedestal fuelling has not been investigated in detail and requires further analysis. In EDGE2D-EIRENE, the grid on which the fluid equations are solved (EDGE2D grid) does not extend

to the limiters. Thus, the simulation of main chamber recycling requires assumptions on the incidence ion flux. We used a projection algorithm that results in all the ion flux arriving at the edge of the plasma grid being recycled in the main chamber. In the simulations presented in this work, the source of neutrals crossing the separatrix was very much dominated by main chamber recycling. Neutrals recycled in the divertor were found to contribute much less to the pedestal fuelling even in the simulations with low particle transport coefficients. The choice of the projection algorithm possibly contributes to this behaviour. In reality, some of the ion flux arriving to the edge of the EDGE2D grid may arrive at the divertor target before it would hit the main chamber limiters. A different projection algorithm that redirects some fraction of the ion flux to recycle at the divertor target (for e.g. exponential fall off with an exponentially decreasing fraction going to the target) would be expected to affect the contribution from the divertor recycling to pedestal fuelling. But due to the lack of experimental constraints, the choice of the projection algorithm is somewhat arbitrary. Further analysis focusing on the ratio of main chamber and divertor recycling would require the edge transport simulation codes that allow for extended plasma grids, covering the whole vessel and thus is outside the scope of this paper. In our simulations, the total amount of pedestal fuelling is experimentally constrained, but the balance between divertor and main chamber recycling is not studied. It is also important to note that the inner divertor in the simulations would be colder and more opaque if cross-field drifts were turned on, thus contributing significantly more to the fuelling of the pedestal [72].

Recently, exceptional progress has been made in pedestal gyrokinetic studies [12, 73–79]. These analyses have identified various micro-instabilities to be potentially responsible for plasma transport in the H-mode pedestal. However, the focus was mostly on the understanding of the pedestal heat transport. Our work has shown that in general, inter-ELM turbulent particle transport plays an important role in setting the density pedestal. Thus, the study of micro-instabilities responsible for particle transport at the edge is a worthwhile line of future work towards a fully predictive pedestal model. Interpretative edge-SOL modelling, such as those presented in this paper, or more direct information about the particle source in the form of neutral density measurements where possible [80–83] could provide information for gyrokinetic simulations to include a realistic particle source term and such advance the understanding of the density pedestal formation.

Data availability statement


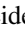
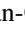








The data that support the findings of this study are available upon reasonable request from the authors.

Acknowledgments

The first author would like to thank A Chankin for fruitful discussions. This work has been carried out within the

framework of the EUROfusion Consortium, funded by the European Union via the Euratom Research and Training Programme (Grant Agreement No. 101052200—EUROfusion) and from the EPSRC [Grant Number EP/W006839/1]. To obtain further information on the data and models underlying this paper please contact PublicationsManager@ukaea.uk. Views and opinions expressed are however those of the authors only and do not necessarily reflect those of the European Union or the European Commission. Neither the European Union nor the European Commission can be held responsible for them.

ORCID iDs

L Horvath  <https://orcid.org/0000-0002-5692-6772>
 J Karhunen  <https://orcid.org/0000-0001-5443-518X>
 P A Schneider  <https://orcid.org/0000-0001-7257-3412>
 J Simpson  <https://orcid.org/0000-0002-0083-9637>
 B Chapman-Oplopoiou  <https://orcid.org/0000-0001-9879-2285>
 L Frassinetti  <https://orcid.org/0000-0002-9546-4494>
 M Groth  <https://orcid.org/0000-0001-7397-1586>
 K Lawson  <https://orcid.org/0000-0002-1251-6392>
 C F Maggi  <https://orcid.org/0000-0001-7208-2613>
 R B Morales  <https://orcid.org/0000-0003-0667-3356>
 O Myatra  <https://orcid.org/0000-0002-1469-2429>
 S Saarela  <https://orcid.org/0000-0002-6838-2194>
 M Vécsei  <https://orcid.org/0000-0003-4596-1211>

References

- [1] Wagner F *et al* 1982 Regime of improved confinement and high beta in neutral-beam-heated divertor discharges of the ASDEX tokamak *Phys. Rev. Lett.* **49** 1408–12
- [2] Greenwald M *et al* 1997 H mode confinement in Alcator C-Mod *Nucl. Fusion* **37** 793–807
- [3] Horton L D, Christiansen J P, Lingertat J, Maggi C F, Mertens V, Pogutse O, Saibene G, Sartori R, Stober J and Suttrop W (The JET Team and the ASDEX Upgrade Team) 1999 Performance near operational boundaries *Plasma Phys. Control. Fusion* **41** B329–41
- [4] Maggi C F *et al* (The ASDEX Upgrade Team, The JT-60U Team and EFDA-JET Contributors for the Pedestal, Edge Physics and the Steady State Operation Topical Groups of the ITPA) 2007 Characteristics of the H-mode pedestal in improved confinement scenarios in ASDEX Upgrade, DIII-D, JET and JT-60U *Nucl. Fusion* **47** 535
- [5] Mantica P *et al* 2011 Ion heat transport studies in JET *Plasma Phys. Control. Fusion* **53** 124033
- [6] Zohm H 1996 Edge localized modes (ELMs) *Plasma Phys. Control. Fusion* **38** 105
- [7] Zohm H 2014 *Magnetohydrodynamic Stability of Tokamaks* (New York: Wiley)
- [8] Snyder P B, Wilson H R, Ferron J R, Lao L L, Leonard A W, Osborne T H, Turnbull A D, Mossessian D, Murakami M and Xu X Q 2002 Edge localized modes and the pedestal: a model based on coupled peeling-ballooning modes *Phys. Plasmas* **9** 2037–43
- [9] Wilson H R, Snyder P B, Huysmans G T A and Miller R L 2002 Numerical studies of edge localized instabilities in tokamaks *Phys. Plasmas* **9** 1277–86

- [10] Dickinson D, Roach C M, Saarelma S, Scannell R, Kirk A and Wilson H R 2012 Kinetic instabilities that limit beta in the edge of a tokamak plasma: a picture of an H-mode pedestal *Phys. Rev. Lett.* **108** 135002
- [11] Saarelma S, Beurskens M N A, Dickinson D, Frassinetti L, Leyland M J and Roach C M (EFDA-JET Contributors) 2013 MHD and gyro-kinetic stability of JET pedestals *Nucl. Fusion* **53** 123012
- [12] Kotschenreuther M et al 2019 Gyrokinetic analysis and simulation of pedestals to identify the culprits for energy losses using ‘fingerprints’ *Nucl. Fusion* **59** 096001
- [13] Viezzer E et al 2017 Investigation of inter-ELM ion heat transport in the H-mode pedestal of ASDEX upgrade plasmas *Nucl. Fusion* **57** 022020
- [14] Viezzer E et al 2018 Ion heat transport dynamics during edge localized mode cycles at ASDEX upgrade *Nucl. Fusion* **58** 026031
- [15] Mordijck S 2020 Overview of density pedestal structure: role of fueling versus transport *Nucl. Fusion* **60** 082006
- [16] Snyder P B, Groebner R J, Leonard A W, Osborne T H and Wilson H R 2009 Development and validation of a predictive model for the pedestal height *Phys. Plasmas* **16** 056118
- [17] Snyder P B, Groebner R J, Hughes J W, Osborne T H, Beurskens M, Leonard A W, Wilson H R and Xu X Q 2011 A first-principles predictive model of the pedestal height and width: development, testing and ITER optimization with the EPED model *Nucl. Fusion* **51** 103016
- [18] Saarelma S, Challis C D, Garzotti L, Frassinetti L, Maggi C F, Romanelli M and Stokes C (JET Contributors) 2017 Integrated modelling of H-mode pedestal and confinement in JET-ILW *Plasma Phys. Control. Fusion* **60** 014042
- [19] Saarelma S, Frassinetti L, Bilkova P, Challis C D, Chankin A, Fridström R, Garzotti L, Horvath L and Maggi C F 2019 Self-consistent pedestal prediction for JET-ILW in preparation of the DT campaign *Phys. Plasmas* **26** 072501
- [20] Luda T, Angioni C, Dunne M G, Fable E, Kallenbach A, Bonanomi N, Schneider P A, Siccino M and Tardini G 2020 Integrated modeling of ASDEX upgrade plasmas combining core, pedestal and scrape-off layer physics *Nucl. Fusion* **60** 036023
- [21] Burckhart A, Wolfrum E, Fischer R, Lackner K and Zohm H (The ASDEX Upgrade Team) 2010 Inter-ELM behaviour of the electron density and temperature pedestal in ASDEX Upgrade *Plasma Phys. Control. Fusion* **52** 105010
- [22] Laggner F M, Wolfrum E, Cavedon M, Dunne M G, Birkenmeier G, Fischer R, Willensdorfer M and Aumayr F (The EUROfusion MST1 Team and The ASDEX Upgrade Team) 2018 Plasma shaping and its impact on the pedestal of ASDEX Upgrade: edge stability and inter-ELM dynamics at varied triangularity *Nucl. Fusion* **58** 046008
- [23] Reiter D 1992 Progress in two-dimensional plasma edge modelling *J. Nucl. Mater.* **196–198** 80–89
- [24] Simonini R, Corrigan G, Radford G, Spence J and Taroni A 1994 Models and numerics in the multi-fluid 2-D edge plasma code EDGE2D/U *Contrib. Plasma Phys.* **34** 368–73
- [25] Wiesen S 2006 EDGE2D/EIRENE code interface report *IRC Report*
- [26] Saibene G et al 1999 The influence of isotope mass, edge magnetic shear and input power on high density ELMy h modes in JET *Nucl. Fusion* **39** 1133–56
- [27] Saibene G et al 2002 Improved performance of ELMy h-modes at high density by plasma shaping in JET *Plasma Phys. Control. Fusion* **44** 1769–99
- [28] Challis C D et al (JET Contributors) 2015 Improved confinement in JET high beta plasmas with an ITER-like wall *Nucl. Fusion* **55** 053031
- [29] Maggi C F et al (JET Contributors) 2015 Pedestal confinement and stability in JET-ILW ELMy H-modes *Nucl. Fusion* **55** 113031
- [30] Suttrop W, Gruber O, Kurzan B, Murmann H D, Neuhauser J, Schweinzer J, Stober J and Treutterer W (The ASDEX Upgrade Team) 2000 Effect of plasma shape variation on ELMs and H-mode pedestal properties in ASDEX upgrade *Plasma Phys. Control. Fusion* **42** A97–A102
- [31] Dunne M G et al 2016 Global performance enhancements via pedestal optimisation on ASDEX upgrade *Plasma Phys. Control. Fusion* **59** 025010
- [32] Schneider P A et al (The ASDEX Upgrade Team, The EUROfusion MST1 Team and JET Contributors) 2021 The dependence of confinement on the isotope mass in the core and the edge of AUG and JET-ILW H-mode plasmas *Nucl. Fusion* **62** 026014
- [33] Osborne T H et al 2000 The effect of plasma shape on H-mode pedestal characteristics on DIII-D *Plasma Phys. Control. Fusion* **42** A175–84
- [34] Leonard A W, Groebner R J, Osborne T H and Snyder P B 2008 Influence of global beta, shape and rotation on the H-mode pedestal structure in DIII-D *Phys. Plasmas* **15** 056114
- [35] Urano H, Kamada Y, Shirai H, Takizuka T, Kubo H, Hatae T and Fukuda T 2001 Thermal energy confinement of high-triangularity ELMy H-mode plasmas in JT-60U *Plasma Phys. Control. Fusion* **44** 11–21
- [36] Snyder P B and Wilson H R 2003 Ideal magnetohydrodynamic constraints on the pedestal temperature in tokamaks *Plasma Phys. Control. Fusion* **45** 1671–87
- [37] Snyder P B, Wilson H R, Osborne T H and Leonard A W 2004 Characterization of peeling–ballooning stability limits on the pedestal *Plasma Phys. Control. Fusion* **46** A131–41
- [38] Snyder P B, Wilson H R, Ferron J R, Lao L L, Leonard A W, Mossessian D, Murakami M, Osborne T H, Turnbull A D and Xu X Q 2004 ELMs and constraints on the H-mode pedestal: peeling–ballooning stability calculation and comparison with experiment *Nucl. Fusion* **44** 320–8
- [39] de la Luna E et al 2015 Understanding the physics of ELM pacing via vertical kicks in JET in view of ITER *Nucl. Fusion* **56** 026001
- [40] Chapman I T et al 2016 Advances in understanding and utilising ELM control in JET *Plasma Phys. Control. Fusion* **58** 014017
- [41] Degeling A W, Martin Y R, Lister J B, Villard L, Dokouka V N, Lukash V E and Khayrutdinov R R 2003 Magnetic triggering of ELMs in TCV *Plasma Phys. Control. Fusion* **45** 1637–55
- [42] Lang P T et al (ASDEX Upgrade Team) 2004 Frequency control of type-i ELMs by magnetic triggering in ASDEX upgrade *Plasma Phys. Control. Fusion* **46** L31–L39
- [43] Pasqualotto R, Nielsen P, Gowers C, Beurskens M, Kempenaars M, Carlstrom T and Johnson D (JET-EFDA Contributors) 2004 High resolution Thomson scattering for Joint European Torus (JET) *Rev. Sci. Instrum.* **75** 3891–3
- [44] Andrew Y, Hawkes N C and Crombe K (JET EFDA Contributors) 2006 Improved charge exchange spectroscopy on the Joint European Torus for ion temperature and rotation velocity profiles *Rev. Sci. Instrum.* **77** 10E913
- [45] Delabie E, Hawkes N, Biewer T M and O’Mullane M G 2016 *In situ* wavelength calibration of the edge CXS spectrometers on JET *Rev. Sci. Instrum.* **87** 11E525
- [46] Scannell R, Beurskens M, Carolan P G, Kirk A, Walsh M, O’Gorman T and Osborne T H 2011 Deconvolution of Thomson scattering temperature profiles *Rev. Sci. Instrum.* **82** 053501
- [47] Huysmans G T A, Goedbloed J P and Kerner W 1991 Isoparametric bicubic Hermite elements for solution of the

- Grad-Shafranov equation *Proc. CP90 Conf. on Computational Physics* vol 02 pp 371–6
- [48] Miller R L, Chu M S, Greene J M, Lin-Liu Y R and Waltz R E 1998 Noncircular, finite aspect ratio, local equilibrium model *Phys. Plasmas* **5** 973–8
- [49] Redl A, Angioni C, Belli E and Sauter O 2021 A new set of analytical formulae for the computation of the bootstrap current and the neoclassical conductivity in tokamaks *Phys. Plasmas* **28** 022502
- [50] Réfy D I, Brix M, Gomes R, Tál B, Zoletnik S, Dunai D, Kocsis G, Kálvin S and Szabolcs T 2018 Sub-millisecond electron density profile measurement at the jet tokamak with the fast lithium beam emission spectroscopy system *Rev. Sci. Instrum.* **89** 043509
- [51] Weisen H, Zabolotsky A, Maslov M, Beurskens M, Giroud C and Mazon D (JET-EFDA Contributors) 2006 Scaling of density peaking in JET H-modes and implications for ITER *Plasma Phys. Control. Fusion* **48** A457–66
- [52] Angioni C, Fable E, Greenwald M, Maslov M, Peeters A G, Takenaga H and Weisen H 2009 Particle transport in tokamak plasmas, theory and experiment *Plasma Phys. Control. Fusion* **51** 124017
- [53] Loarte A, Leyland M J, Mier J A, Beurskens M N A, Nunes I, Parail V, Lomas P J, Saibene G R, Sartori R I A and Frassinetti L 2013 Plasma density and temperature evolution following the H-mode transition at JET and implications for ITER *Nucl. Fusion* **53** 083031
- [54] Szepesi G, Appel L C, de la Luna E, Frassinetti L, Gaudio P, Gelfusa M, Gerasimov S, Hawkes N C, Sertoli M and Terranova D (JET Contributors) 2021 Advanced equilibrium reconstruction for JET with EFIT++ *47th EPS Conf. on Plasma Physics* p 3.1037
- [55] Challis C D, Cordey J G, Hamnén H, Stubberfield P M, Christiansen J P, Lazzaro E, Muir D G, Stork D and Thompson E 1989 Non-inductively driven currents in JET *Nucl. Fusion* **29** 563–70
- [56] Horvath L *et al* (JET Contributors) 2021 Isotope dependence of the type I ELMy H-mode pedestal in JET-ILW hydrogen and deuterium plasmas *Nucl. Fusion* **61** 046015
- [57] Matthews G F *et al* (The ITER-like Wall Project Team) 2007 Overview of the ITER-like wall project *Phys. Scr.* **T128** 137–43
- [58] Karhunen J *et al* 2019 Effect of reflections on 2d tomographic reconstructions of filtered cameras and on interpreting spectroscopic measurements in the jet iter-like wall divertor *Rev. Sci. Instrum.* **90** 103504
- [59] Giroud C, Meakins A, Carr M, Baciero A and Bertrand C 2018 CHERAB spectroscopy modelling framework (<https://doi.org/10.5281/zenodo.1206142>)
- [60] Carr M *et al* 2017 Towards integrated data analysis of divertor diagnostics with ray-tracing *44th EPS Conf. on Plasma Physics* p O5.130
- [61] Meakins A and Carr M 2019 Raysect/source: Release 0.5.5 (<https://doi.org/10.5281/zenodo.2583254>)
- [62] Summers H P, Dickson W J, Mullane M G O, Badnell N R, Whiteford A D, Brooks D H, Lang J, Loch S D and Griffin D C 2006 Ionization state, excited populations and emission of impurities in dynamic finite density plasmas: I. the generalized collisional–radiative model for light elements *Plasma Phys. Control. Fusion* **48** 263–93
- [63] de la Cal E *et al* 2020 Impact of divertor configuration on recycling neutral fluxes for ITER-like wall in JET H-mode plasmas *Plasma Phys. Control. Fusion* **62** 035006
- [64] Belli E A and Candy J 2008 Kinetic calculation of neoclassical transport including self-consistent electron and impurity dynamics *Plasma Phys. Control. Fusion* **50** 095010
- [65] Belli E A and Candy J 2012 Full linearized Fokker-Planck collisions in neoclassical transport simulations *Plasma Phys. Control. Fusion* **54** 015015
- [66] Belli E A, Hammett G W and Dorland W 2008 Effects of plasma shaping on nonlinear gyrokinetic turbulence *Phys. Plasmas* **15** 092303
- [67] Marinoni A, Brunner S, Camenen Y, Coda S, Graves J P, Lapillonne X, Pochelon A, Sauter O and Villard L 2009 The effect of plasma triangularity on turbulent transport: modeling TCV experiments by linear and non-linear gyrokinetic simulations *Plasma Phys. Control. Fusion* **51** 055016
- [68] Beeke O, Barnes M, Romanelli M, Nakata M and Yoshida M 2021 Impact of shaping on microstability in high-performance tokamak plasmas *Nucl. Fusion* **61** 066020
- [69] Hughes J W, LaBombard B, Mossessian D A, Hubbard A E, Terry J and Biewer T (The Alcator C-Mod Team) 2006 Advances in measurement and modeling of the high-confinement-mode pedestal on the alcator c-mod tokamak *Phys. Plasmas* **13** 056103
- [70] Hughes J W, LaBombard B, Terry J, Hubbard A and Lipschultz B 2007 Edge profile stiffness and insensitivity of the density pedestal to neutral fuelling in alcator c-mod edge transport barriers *Nucl. Fusion* **47** 1057–63
- [71] Reksoatmodjo R, Mordijck S, Hughes J W, Lore J D and Bonnin X 2021 The role of edge fuelling in determining the pedestal density in high neutral opacity alcator c-mod experiments *Nuclear Materials and Energy* **27** 100971
- [72] Groth M *et al* 2011 Poloidal distribution of recycling sources and core plasma fuelling in DIII-D, ASDEX-Upgrade and JET L-mode plasmas *Plasma Phys. Control. Fusion* **53** 124017
- [73] Hatch D R, Kotschenreuther M, Mahajan S, Valanju P, Jenko F, Told D, Görler T and Saarelma S 2016 Microtearing turbulence limiting the JET-ILW pedestal *Nucl. Fusion* **56** 104003
- [74] Hatch D R, Kotschenreuther M, Mahajan S, Valanju P and Liu X 2017 A gyrokinetic perspective on the JET-ILW pedestal *Nucl. Fusion* **57** 036020
- [75] Kotschenreuther M, Hatch D R, Mahajan S, Valanju P, Zheng L and Liu X 2017 Pedestal transport in H-mode plasmas for fusion gain *Nucl. Fusion* **57** 064001
- [76] Hatch D R *et al* (JET Contributors) 2019 Direct gyrokinetic comparison of pedestal transport in JET with carbon and ITER-like walls *Nucl. Fusion* **59** 086056
- [77] Parisi J F, Parra F I, Roach C M, Giroud C, William Dorland D R, Hatch M B, Hillesheim J C, Aiba N, Ball J and Ivanov P G (JET Contributors) 2020 Toroidal and slab ETG instability dominance in the linear spectrum of JET-ILW pedestals *Nucl. Fusion* **60** 126045
- [78] Hatch D R *et al* (JET Contributors) 2021 Microtearing modes as the source of magnetic fluctuations in the JET pedestal *Nucl. Fusion* **61** 036015
- [79] Chapman-Oploupoiou B *et al* 2022 The role of ETG modes in JET-ILW pedestals with varying levels of power and fuelling *Nucl. Fusion* **62** 086028
- [80] Rosenthal A M *et al* 2021 A 1D Lyman-alpha profile camera for plasma edge neutral studies on the DIII-D tokamak *Rev. Sci. Instrum.* **92** 033523
- [81] Laggner F M, Bortolon A, Rosenthal A M, Wilks T M, Hughes J W, Freeman C, Golfinopoulos T, Nagy A, Mauzey D and Shafer M W 2021 Absolute calibration of the Lyman-alpha measurement apparatus at DIII-D *Rev. Sci. Instrum.* **92** 033522
- [82] Rosenthal A M *et al* 2021 Calculation of pedestal transport using direct measurements of neutral emissivity on DIII-D *25th Joint EU-US Transport Task Force Meeting*
- [83] Sciortino F *et al* 2021 Experimental inference of neutral and impurity transport in Alcator C-Mod using high-resolution X-ray and ultra-violet spectra *Nucl. Fusion* **61** 126060